Stochastic Simulation of Aerosol Deposition in Model Filters

Aerosol deposition in model filters composed of layers of parallel fibers with the orientation of the fiber of each layer kept arbitrary was simulated stochastically. Particle positions at the inlet of the filter were assumed to be randomly distributed over the inlet plane with the trajectory assumed to be rectilinear because of the particles' high inertia. In the simulation, the track of each particle through the filter was monitored and the possible bounce-off from collision surfaces was allowed for. Deposition behavior and the structure of deposits were studied with various aerosol flow conditions and filter characteristics.

B. V. Ramarao, Chi Tien
Department of Chemical Engineering
and Materials Science
Syracuse University
Syracuse, NY 13244

Introduction

The dynamic behavior of aerosol deposition is characterized by the time histories of collection efficiency and the pressure drop across the fibrous filter. The collection efficiency and pressure drop of a filter remain steady in the initial period of filtration. As time passes, the filter becomes increasingly loaded with deposited aerosols, and the fibers are no longer clean. At this point, aerosol deposits adhering to the fibers act as additional collection surfaces and consequently the collection efficiency starts to increase. The collection efficiency rises rapidly as additional deposits form until eventually the filter clogs and a thick, porous filter cake forms.

The pressure drop across the filter shows a similar behavior. Initially, when the fibers are relatively clean, the pressure drop across the filter remains essentially constant with time. However, as the dust loading increases in the filter, the collection surfaces become covered with deposits and the pressure drop begins to increase. This increase becomes significant as the filter becomes nearly clogged. In many practical situations the point at which a filtration operation is stopped is often determined by the pressure drop increase.

Most studies of aerosol filtration have been limited to the initial period of filtration when the collection surfaces (fibers in fibrous filters, filter grains in granular beds, etc.) are clean. Numerous correlations are available to predict the collection efficiency that results from different mechanisms in either fibrous or granular filters (Davies, 1973).

Only recently has some attention been given to studies of filtration when the deposition is significant. Billings (1966) found that when a single fiber was exposed to aerosols, it started collecting particles to form chainlike deposits, commonly called dendrites. After a certain amount of deposition occurred, most collection took place on the previously deposited particles. The collection efficiency was found to be a monotonically increasing function of the number of deposited particles.

The growth of particle dendrites has been studied by Payatakes and Tien (1976) and by Payatakes and Gradon (1980). Payatakes and Tien modeled dendrite growth by considering the evolution of what were called ideal dendrites, that is, chains of particles strung in a straight line. Recently, Emi et al. (1982) examined the effect of particle loading in filters composed of wire-mesh screens by determining experimentally how the collection efficiency and the pressure drop of the filter varied with the extent of deposition. Walata et al. (1986) undertook a similar study to investigate the loading effect in granular filters.

A conceptually simple and direct way of studying aerosol filtration is to construct computer experiments to simulate the trajectories of aerosols as they flow through a filter. Such experiments are based on the principles developed by Tien and coworkers (Tien et al., 1977; Wang et al., 1977; Beizaie et al., 1981). Such an approach was adopted also by Pendse and Tien (1982) to study aerosol filtration in granular beds and by Tsiang et al. (1982) for aerosol filtration in model fibrous filters.

The model filters used in the work of Tsiang et al. consisted of a single layer of parallel cylindrical fibers, with the fiber axes normal to the direction of flow. One of the most important findings in that work is the effect of bounce-off of impacting particles. It was found that at high gas velocities, particle bounce-off became significant. Experiment and simulation were seen to agree only if this effect was properly considered in the simulation.

The present study represents a generalization of the earlier work of Tsiang et al. (1982). The model filters considered in this

work are composed of multiple layers of parallel fibers instead of a single layer. Furthermore, the orientation of each layer with respect to the direction of aerosol flow is assumed to be random, as shown in Figure 1. In the special case in which the adjacent fiber layers are placed at right angles on top of each other, the model filter can be considered as one composed of wire-mesh screens.

Simulation Principles

The basic principles used in this stochastic simulation are the same as those previously formulated by Tien et al. (1977):

1. Aerosol particles enter the filter one at a time. One may explain this more precisely by stating that the probability of more than one particle entering the filter at exactly the same time is much less than that of a single particle entering.
2. The positions of the entering aerosol particles (at the inlet of the filter) are randomly distributed.

The simulation is conceptually simple and straightforward. Knowing the inlet position of the aerosol particle, one then knows its trajectory. The trajectory can, in turn, be used to determine whether or not the particle will impact either any filter fibers or any of the previously deposited particles. Based on the bounce-off criteria, to be discussed later, one may then predict whether the particle will be collected or bounced off. If the particle will be collected, its position in the collected state is recorded. In the event of bounce-off, the particle trajectory will again be monitored until the particle is either collected or flows out of the filter.

In the following sections, we present the various procedures developed for implementing the above principles.

Determination of particle trajectories

Like Pendse and Tien (1982), we assume that because of high inertia, particle trajectories are rectilinear and are determined by the initial direction of the particles. Assuming that all aerosols enter the filter along that filter's axial direction, the initial segment of any particle trajectory (that is, before its impact on fibers or previously deposited aerosols) is rectilinear along the direction of aerosol flow. The trajectory of any reflected particle can be determined by its incidence direction as well as by its material characteristics. Accordingly, for a given particle, once one knows its initial position at the inlet (or the control surface used in the simulation), one may also determine its trajectory through the filter.

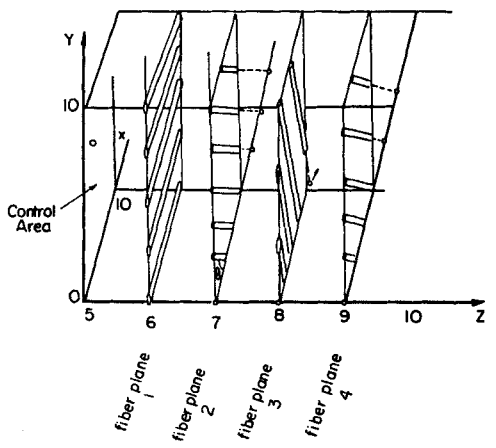

Figure 1. Multilayered model filter considered in simulation.

Collision dynamics and bounce-off

In fibrous filtration of aerosols, when an aerosol particle impacts a fiber or a previously deposited particle, the particle may either be collected or bounced off. A simple analysis of the collison–bounce-off phenomenon based on the work of Dahneke (1971) is given below.

When a particle approaches a collection surface, attractive forces between the particle and the surface start to develop and serve to effect the adhesion of the particle to the surface. The attractive forces give rise to a "well" in the potential energy of the particles. The kinetic energy due to the velocity component parallel to the surface may be assumed to be conserved.

Consider a particle approaching the surface with the normal velocity component V_{ni}; the kinetic energy resulting from this velocity is KE_{ni}. Let V_{nr} denote the velocity upon bounce-off and KE_{nr} the resulting kinetic energy. An energy balance before and after collision gives

$$KE_{nr} = (KE_{ni} + E_i)e^2 - E_r \tag{1}$$

where E_i and E_r denote the potential energy wells created by the attractive surface forces; m, the mass of the particles; and e, the coefficient of restitution, which is unity for a perfectly elastic collision. Notice that by multiplying the incident total energy by the coefficient of restitution, e, we have accounted for the possible loss of energy during the collision process.

Equation 1 can be used to obtain the condition leading to particle deposition. By letting KE_{nr} equal zero, a lower limit of KE_{ni}, below which particle bounce-off will not occur, can be obtained from Eq. 1. Assuming that $E_i = E_r = E_w$, the corresponding normal component, V_{cr}, is found to be

$$V_{cr} = \left[\frac{2E_w(1 - e^2)}{me^2}\right]^{1/2} \tag{2}$$

For the case of collisions of two spheres, m is replaced by the reduced mass. The coefficient of restitution can be correlated as shown by Dahneke (1971) as

$$e = e_o + \exp(-1.7\lambda) - 1 \tag{3}$$

where e_o is the zero velocity limit of e and is equal to 0.965 and λ is known as the inelasticity parameter. The inelasticity parameter is a function of the various material constants and is

$$\lambda = \frac{2}{3\pi^{2/5}}\left(\frac{d_p}{d_f}\right)^2 \frac{1}{\left(1 + \frac{d_p}{d_f}\right)^{1/10}}\left(\frac{V_{ni}}{v_f'}\right)^{1/5}\left(\frac{\rho_p}{\rho_f}\right)^{3/5}\left(\frac{k_f}{k_p + k_f}\right)^{2/5} \tag{4}$$

for the case of a sphere-cylinder collision, and was assumed to be

$$\lambda = \frac{(2)^{5/10}}{3\pi^{2/5}}\left(\frac{V_{ni}}{v_f'}\right)^{1/5} \tag{5}$$

for the case of a sphere-sphere collision.

The inelasticity parameter determines the velocity after reflection by acounting for energy dissipation during the collision. The above correlations were first suggested by Dahneke to account for energy dissipation mechanisms involving flexural work associated with bulk displacement of the body. The fiber and particle diameters are denoted by d_f and d_p; v_f and v_p are the Poisson ratios of the fiber and the particle; ρ_f and ρ_p are the densities of the fiber and the particle. v_i', k_f, and k_p are appropriate functions of the material constants of the fiber and particle as shown in Table 1. This equation was also used to estimate the inelasticity parameter for the sphere-sphere collisions, with appropriate changes in the material constants. The depth of the potential well for the sphere-cylinder case is given by

$$E_w = \frac{A}{12z_o} \frac{d_p}{\left(1 + \frac{d_p}{d_f}\right)^{1/2}} \tag{6}$$

whereas that for the case of two identical spheres adhering to each other is given by

$$E_w = \frac{Ad_p}{24z_o} \tag{7}$$

where A is the Hamaker constant and z_o is the equilibrium separation distance of the two spheres. The various symbols are also defined in Table 1.

In the event of particle bounce-off, the magnitude of the reflected velocity, V_{nr}, is found by approximating

$$V_{nr} \approx eV_{ni} \tag{8}$$

and the direction of the particle trajectory is found from Snell's law, as shown in Figure 2. The tangential velocity components V_{ti} and V_{tr} for the incident and reflected particles are assumed to be equal. This is a consequence of assuming that only the kinetic energy due to the tangential component of the velocity is conserved during the collision, as stated earlier.

Equation 2 can be used to determine V_{cr} as a function of particle diameter for a given fiber size and a specific set of material

Table 1. Aerosol and Filter Characteristics

	Aerosol Particles
Density, ρ_p	1.0 g/cm^3
Diameter, d_p	2.0 μm
Poisson's ratio, v_p	0.33
Young's molulus, Y_p	0.32×10^{11} dyne/cm^2
Velocity, V_∞	3 to 20 cm/s
	Filter
Fibers per plane	4 to 6
Fiber spacing	25 μm
Interlayer spacing	10 μm
Total fiber projected area	40 μm^2
Fiber diameter, d_f	10 μm
Fiber density, ρ_f	7.8 g/cm^3
Poisson's ratio, v_f	0.29
Young's modulus, Y_f	21×10^{11} dyne/cm^2
Separation distance, z_o	4 Å
Hamaker constant, A	10^{-12} erg
$k_i = (1 - v_i^2)/Y_i$ $i = f$ or p	$v_i' = 1/(k_i\rho_i)^{1/2}$

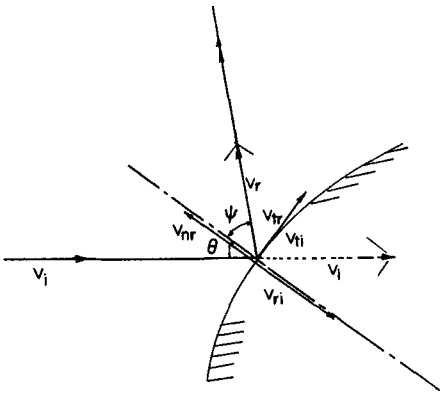

Figure 2. Calculation of particle trajectory after bounce-off.

constants. The calculations, however, can only be done iteratively since e is a function of V_{cr}. In making the calculation, one must also assume values for the separation distance in Eq. 6. The value of $4A$ is typical for a sphere-sphere separation and was used for further calculations.

Table 1 shows a sample set of parameters used to illustrate this calculation. Figure 3 shows how the escape velocity varies with particle diameters. The results were obtained from Eq. 2 using Newton's iterative method. The critical velocity decreases with increasing particle size. Increasing the particle size increases the momentum and kinetic energy carried by the particles; hence, bounce-off can be expected with large particles at the same velocity. This behavior is dependent on the various elastic and material constants of the two surfaces involved.

Program structure

The basic structure underlying the simulation is as follows. We first generate a filter by determining the orientations of the fiber axes of all the layers. Then, the escape velocities for the particle-particle and particle-fiber collisions are determined.

Next, the initial positions of aerosol particles at the filter inlet are determined. According to the general principle previously formulated for simulating particle deposition from suspensions flowing past collectors, it is necessary to set up the control surface from which all approaching particles originate. For filters,

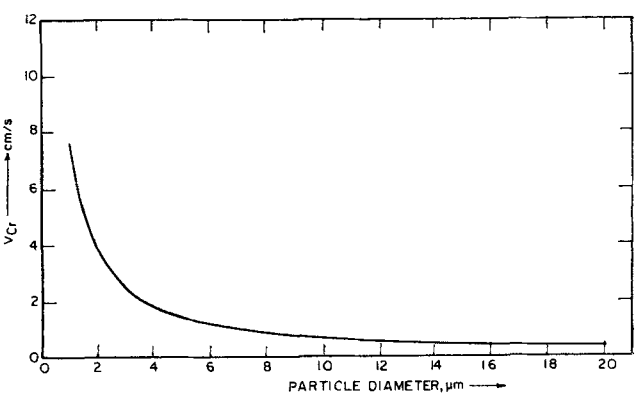

Figure 3. Variation of critical escape velocity with particle size.
Bounce-off from fibers

the control surface should be a representative part of the inlet. Tsiang et al. (1982) in their work chose the control surface to be one normal to the aerosol flow and containing two halves of two adjacent fibers. The proper choice in this work, however, is not so obvious because the orientation of the fiber layers is not regular, but randomly selected.

By trial and error, the control surface was taken to be a square with a dimension of four times the interfiber distance. This choice gives us, in essence, a filter cross-sectional area equal to that of the control surface.

Once the control surface is determined, and with the initial positions known, the initial trajectory of the particles can be determined easily, since the x and y coordinates of the trajectory are independent of its axial position (z coordinate). Figure 1 shows the coordinate system. The possibility of a particle impacting upon previously deposited particles or filter fibers is observed by knowing the locations of the fibers and deposited particles. The collision's outcome is determined by the criteria discussed earlier. In the event that particle adhesion occurs, the inventory of deposited particles is updated, and a new approaching particle is considered.

Sometimes a particle may be found to pass through the side walls of the filter. This situation occurs only because in the simulation we consider a representative part of the filter cross section instead of the cross section in its entirety. To account for such particle losses, we reintroduce for each escaping particle a new particle entering at the opposing boundary and with a direction parallel to the escaping particle; see Figure 6a.

The simulation results are in the form of the number of deposited particles, n, vs. the number of approaching particles, N, as well as the deposited particles' positions (which give the morphology of particle deposits). The instantaneous collection efficiency, E, is given as

$$E = \frac{dn}{dN} \cong \frac{\Delta n}{\Delta N} \tag{9}$$

where ΔN represents a suitable increment in the total number of particles considered and Δn is the corresponding number of particles retained by the filter. Note that discretization in this form leads to a small fluctuation in the actual value of the collection efficiency because of the stochastic nature of the simulation. A very small ΔN gives rise to large fluctuations in Δn, and hence in the efficiency. However, a very large ΔN is not truly representative of the instantaneous collection efficiency. Hence, an optimum ΔN needs to be chosen.

Results

Analysis of simulation results

As the simulation is stochastic in nature, the deposition behavior (the relationship of n to N and the deposit structure as a function of time) observed for each set of approaching particles can be viewed as a single outcome of an ensemble of outcomes. The expected behavior can therefore be predicted from the ensemble averages as well as from the statistical properties of the ensemble. In this regard, it is important to determine the minimum size of a sample from which a reasonably accurate ensemble average may be estimated.

A set of simulations was done corresponding to the conditions listed in Table 1 for $V_\infty = 10$ cm/s. From the results of n vs. N,

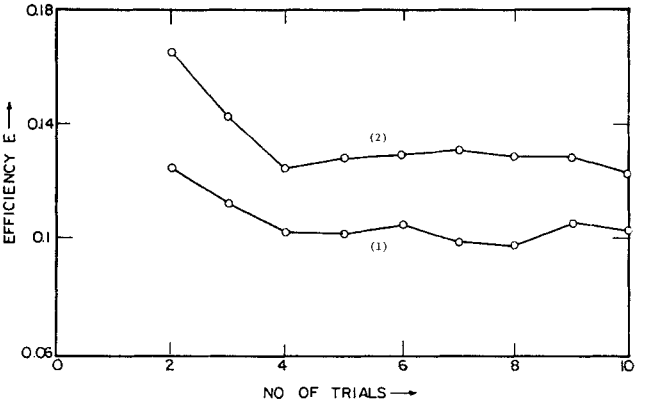

Figure 4. Variation of average collection efficiency with number of trials.
Efficiency monitored after deposition of (1) 200 particles, (2) 400 particles

the value of the collection efficiency up to $N = 2{,}000$ was obtained. Up to fifteen independent trials were carried out. The average values of E for a given number of trials were plotted against the number of trials, as shown in Figure 4. For this set of results, it is obvious that the average value of the efficiency approaches a constant if the number of trials exceeds ten. All the results reported in this work were obtained from a set of at least ten different trials.

Trajectory of a particle through the filter

We tracked a set of particles through a filter consisting of a single layer of parallel fibers along the x axis. The initial particle trajectory (before collision) was constrained to a plane of constant x.

To demonstrate the particle trajectories, consider two adjacent fibers, which in Figure 5 are represented by the top and bottom semicircles. The particle paths through this fiber arrangement are shown as straight lines, with the arrows marking the direction of movement; multiple-headed arrows represent reflected rays. The initial position of the particles was chosen at random. When a particle comes close enough to either of the two fibers, the path was assumed to bounce off an imaginary surface that is one particle radius away from the fiber surface. Notice

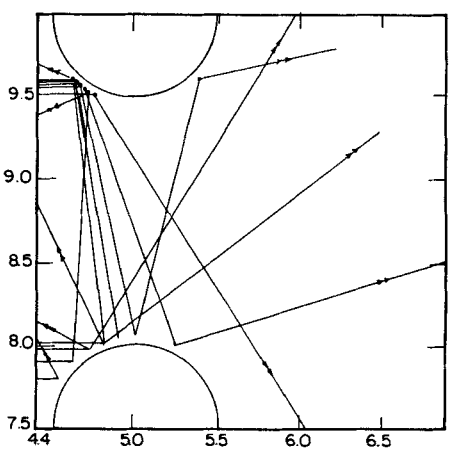

Figure 5. Trajectories through a single layer of filter.

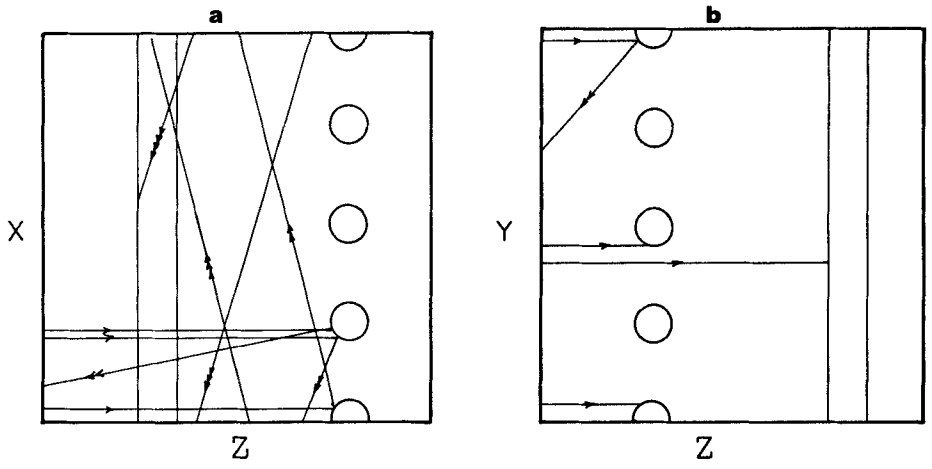

Figure 6. Trajectories through a two-layer filter.

that the program faithfully tracks reflections from each part of the fibers.

The next filter considered in this case was composed of two layers of parallel fibers with the fiber axes coinciding with the x axis (first layer) and the y axis (second layer), respectively. A fraction of the kinetic energy of the particle was dissipated during the collision by flexural work so that the magnitude and direction of the rebound velocity are different from the incident velocity.

The trajectories of a number of particles in such a two-layer filter are shown in Figures 6a and 6b for both the x-z and the y-z planes. A particle entering the filter through the front face is constrained either to be deposited within the filter or to leave only through the rear face by employing reflective boundary conditions. If a particle leaves through any of the side walls of the filter element being considered, it is reintroduced into the cross section at the same location on the opposite face and with the same orientation. This constraint has the effect of reflecting particles from the boundaries and thus allows accounting for particles that the simulation would otherwise lose through the various faces. It accounts for the fact that the filter unit chosen from the simulation has a finite size by introducing suitable periodicity at the boundaries.

Deposit structure

As a sample simulation, we studied the structure of the deposit developed in wire-mesh screen filters consisting of two to four layers. Note that fibers of each successive plane in the filter are oriented horizontally at right angles to the fibers of the preceding plane. Hence, fibers of planes other than the first two do not directly "see" any portion of the aerosol flow. Particles collect on them only as a result of their bouncing off the first two layers.

The deposit structures are shown in Figures 7 through 10. The fibers shown running horizontally in the figures belong to the first and the third layers, the fibers shown running vertically belong to the second and the fourth layers. The results shown in Figure 7 were obtained for a superficial velocity V_∞ of 3 cm/s. At this velocity and corresponding to the conditions given in Table 1, bounce-off from both the fibers and previously deposited particles is nonexistent, since the critical escape velocities are higher than 3 cm/s. This behavior can best be seen if the deposition results are shown in the x-z plane. Deposition appeared only on the first two layers and at the front of the fiber, Figures 7a and 7b.

As the superficial velocity increased from 3 to 5 cm/s, Figure 8, and ultimately to 10 cm/s, Figure 9, the deposit began to penetrate into the third and the fourth layers. In addition, particle collection became more uniform over the entire fiber surface; it was not restricted to the front of the fibers. As the superficial velocity increased, the likelihood of particle bounce-off upon impact increased. Particles bouncing off the front of a fiber may be collected by the rear of the fiber in the preceding layer. The result was more uniform deposition. As time increases, thereby increasing as well the number of particles considered, one can also expect deposition to increase, which can be seen by comparing the results shown in Figure 9 with those in Figure 10.

Simulation of deposition in wire-mesh screens

As stated before, two layers of parallel fibers with their axes placed at right angles on the same plane may be used to approxi-

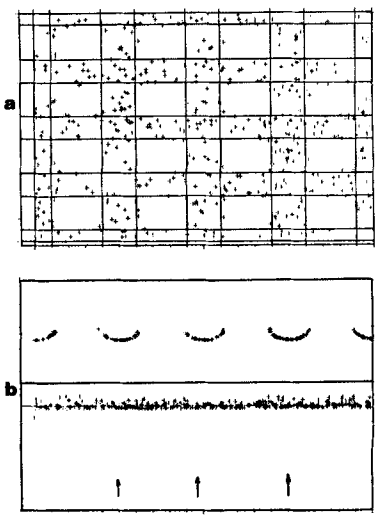

Figure 7. Deposit structure in model filter, low aerosol velocity.

V_∞ = 3 cm/s; N = 2,000

a. Face view of filter; b. Edge view

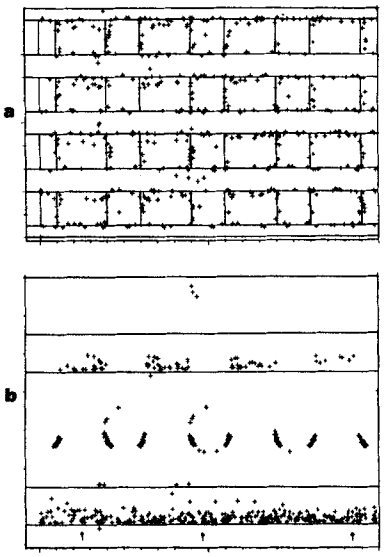

Figure 8. Deposit structure in model filter, intermediate aerosol velocity.

$V_\infty = 5$ cm/s; $N = 2{,}000$
a. Face view of filter; b. Edge view

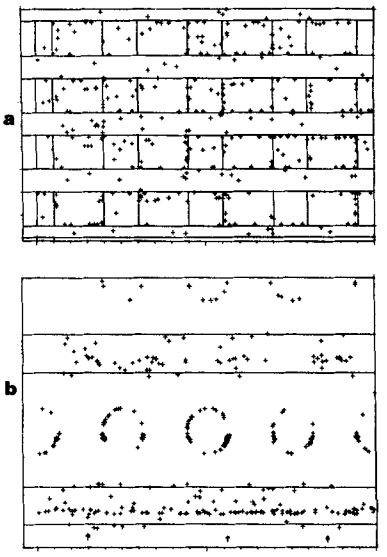

Figure 10. Deposit structure in model filter, buildup with time.

$V_\infty = 10$ cm/s; $N = 3{,}000$

mate a wire-mesh screen. The simulation was carried out by first generating two-layer filters and by then carrying out a number of trials with 2,000 particles for each trial. The aerosol velocity was kept typically at 10 cm/s and the particles were assumed to be 1 μm in radius. The critical velocities determining bounce-off or adhesion were calculated to be 3.97 cm/s for collision against the fibers and 4.67 cm/s for collision against the particles. Other conditions for the simulations are given in Table 1.

The variation of the collection efficiency with the number of particles passing through is shown in Figure 11. Notice that the number of particles is proportional to the dimensionless time that is used to describe aerosol deposit variations. The collection efficiency fluctuates for small steps in time. However, the variations are smoothed by taking larger steps in time.

Notice also the increase in collection efficiency as the particles increase in number. The velocity of the aerosol controls the bounce-off behavior of the particles on the filter. The effect of varying the aerosol velocity on the collection efficiency is shown in Figure 12. When the aerosol velocity is below the critical velocities for bounce-off from the fibers or the particles, all the particles coming into contact with the collector surfaces are deposited. The result is high collection efficiency, as exemplified by the top curve in the figure. The drastic decrease in collection efficiency as velocity increases is illustrated by the other curves in the same figure.

The collection efficiency of the filters containing one, two, three, four, and five layers of fibers was determined successively. The total efficiency of the filter, E, is used to calculate a sin-

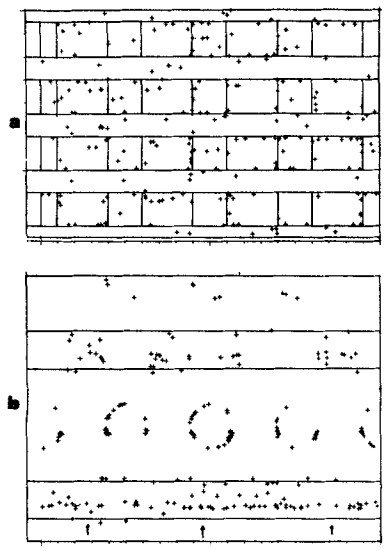

Figure 9. Deposit structure in model filter, high aerosol velocity.

$V_\infty = 10$ cm/s; $N = 2{,}000$
a. Face view of filter; b. Edge view structure

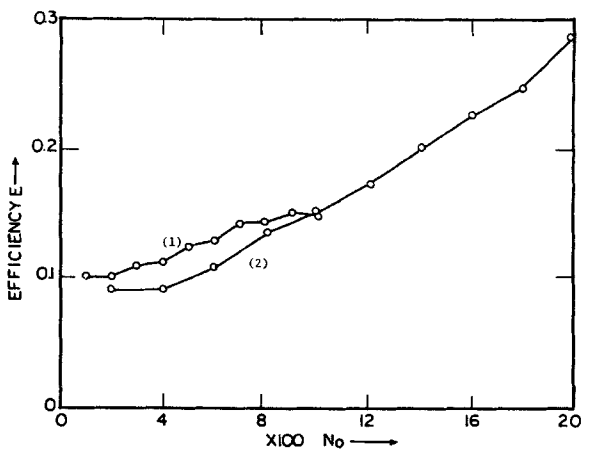

Figure 11. Variation of collection efficiency with number of particles.

Efficiency calculated based on increments of (1) 100 particles, (2) 200 particles.

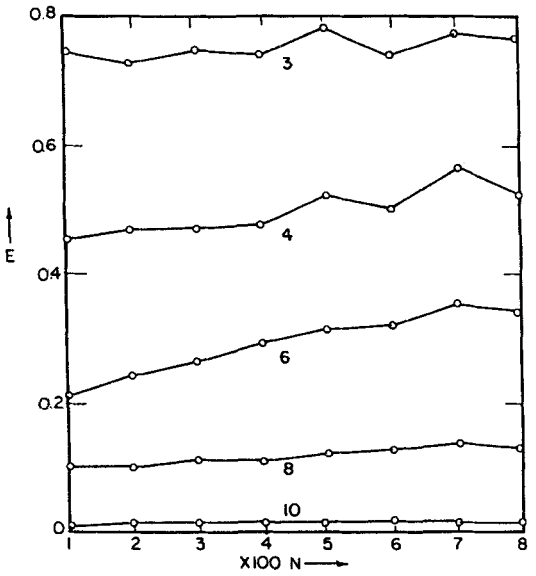

Figure 12. Variation of collection efficiency with aerosol velocity.
Numbers on curves are velocity, V_∞, cm/s

gle-layer efficiency, η_i, as follows:

$$1 - E = (1 - \eta_1)(1 - \eta_2) \ldots (1 - \eta_i) \qquad (10)$$

This single-layer efficiency is displayed in Figure 13 as a function of the number of particles for the various filters. Notice that only the first two layers contribute significantly to collection. The other layers of fibers, being directly behind these two layers, do not significantly enhance deposition.

Increasing particle diameter has two major effects on the collection behavior. The larger diameter contributes to a low escape velocity and hence tends to lower collection efficiency values. On the other hand, collection as a result of interception takes on more importance and in fact dominates collection when the particle size is very high. Figure 14 shows the effect of varying the size of the aerosol particles. Notice that with small sizes, the collection efficiency is relatively flat with time, although the initial collection efficiency values are considerably higher. As particle size increases, the escape velocities decrease drastically, thus lowering the initial collection efficiencies but increasing collection efficiency with loading to a significant level. This behavior is reflected in the distinct upward trends in the lower curves of the figure.

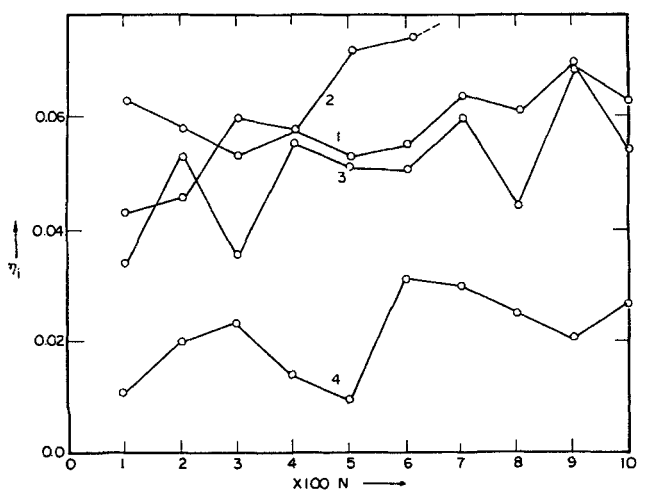

Figure 13. Variation of single-layer efficiency with depth of filter.
Numbers on curves indicate layer number from filter face

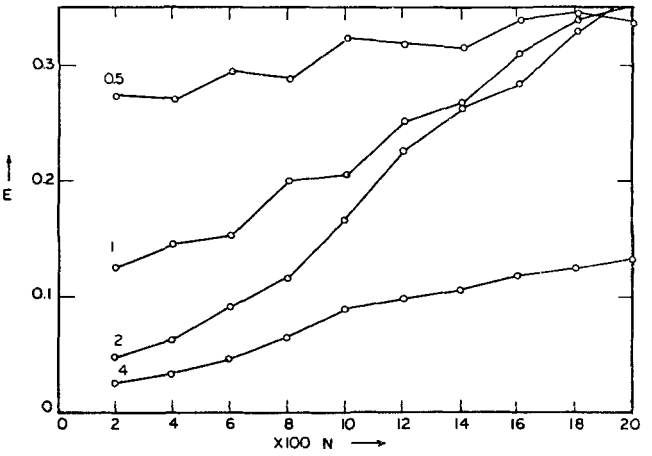

Figure 14. Variation of collection efficiency with particle size.
Numbers on curves are particle diameter, d_p, μm

Applications

In the following section, three examples are presented to demonstrate the potential utility of the simulation procedure in actual aerosol filtration applications.

Initial collection on wire-mesh screens

Consider a model filter composed of two layers of parallel fibers such that the axes of the fibers on one layer lie at right angles across those of the next layer. If the interlayer distance from center to center is d_f, the diameter of the fibers, then the two layers will touch each other. Thus, the model filter may be viewed as approximating a single layer of wire-mesh screen. The clean collector efficiency is

$$E_o = \left(\frac{dn}{dN}\right)_{N=0} \qquad (11)$$

The initial collection efficiency can easily be obtained from geometrical considerations if the particle trajectories are assumed to be rectilinear. A basic element of a wire-mesh screen is an opening in the screen surrounded by four half-wires along its sides. Figure 15 illustrates these characteristics. The collection efficiency is given by

$$E_o = \frac{\text{Area of fibers available for collection}}{\text{Total area of aerosol flow}} \qquad (12)$$

The denominator is simply ℓ^2, where ℓ is the interfiber distance as shown in the figure. The total projected surface area of the four half-fibers corrected for the interception effect as shown is $\ell^2 - (\ell - d_f - d_p)^2$. However, only part of this area is available

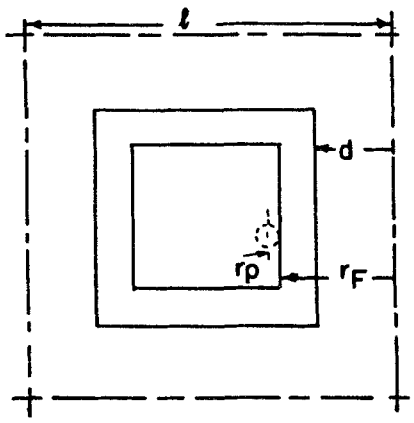

Figure 15. Collection of a unit cell of a wire-mesh screen.
r_F = fiber radius; r_p = particle radius

for collection. As shown in Figure 16, consider aerosol particle impact on a fiber with an incident velocity of V_∞. The normal component of the incident velocity, V_{ni}, varies with the impact point; that is

$$V_{ni} = V_\infty \cos\theta \tag{13}$$

where θ is the angular position of the impact point. Equation 13 shows that V_{ni} decreases as the impact point moves away from the front stagnation point. For a given velocity and given aerosol-fiber combination (which determine the value of V_{cr}), there exists a critical height d_m above which particle collection occurs. It is given as

$$d_m = \frac{(d_f + d_p)}{2} \sin\theta_c \tag{14}$$

$$\theta_c = \cos^{-1}(V_{cr}/V_\infty) \tag{15}$$

The area available for collection is given by $\ell^2 - (\ell - d_f - d_p)^2$.

$$E_o = \frac{(\ell - 2d_m)^2 - (\ell - d_f - d_p)^2}{\ell^2} \tag{16}$$

The results of E_o according to Eq. 16 are displayed in Figure 17. Comparing these results with those obtained from the simulation, one finds the simulation results to be higher than those given by Eq. 16. Nevertheless, they essentially follow the same trend, and the difference is well within 20%.

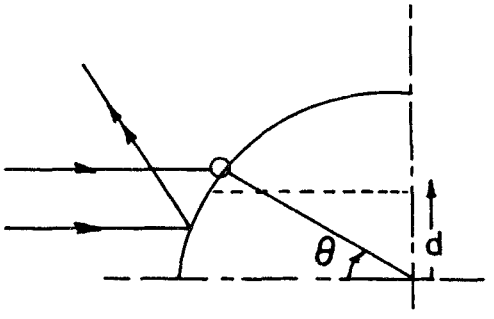

Figure 16. Definition sketch for bounce-off considerations from a fiber of a wire-mesh screen.

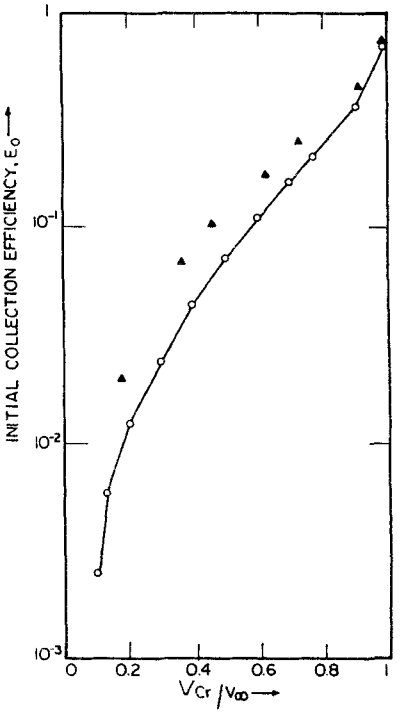

Figure 17. Initial collection efficiency for a wire-mesh screen as a function of aerosol velocity.
▲ Simulation result; O Calculation

Emi et al. (1982) measured collection efficiencies of model filters composed of layers of wire-mesh screens. In Table 2, the efficiencies they reported and the corresponding values calculated from Eq. 16 are shown. It is clear that at low gas velocities (or more appropriately, low Stokes numbers), the difference between the experiment and prediction is significant, being more than one order of magnitude. However, with the increase in gas velocity, the difference diminishes. It is also interesting to note that the collection efficiency predicted from Eq. 16 at high Stokes numbers (approximately 0.01 to 0.05 for N_{St} between 0.1 and 0.3) is similar in magnitude to that obtained in the filtration of aerosols in granular beds (Jung et al., 1987).

Table 2. Comparison of Experimental Results of Emi et al. (1982) with Geometric Calculation of Bounce-Off

	Exp.	Simul.
Fiber radius, μm	12.5	12.5
Interfiber distance, μm	25	25
Particle radius, μm	0.55	0.5
Velocity, cm/s	4 to 110	3 to 120
Stokes No.	Efficiency	
	Exp.	Calc.
0.05	—	0.3
0.1	0.008	0.14
0.15	0.009	0.05
0.2	0.015	0.029
0.3	0.022	0.014

Adhesion probability

The adhesion probability γ is the standard way of describing the effect of particle bounce-off. In terms of the model filters and the high inertia assumption used in this work, the adhesion probability is equal to the ratio provided by the filter for collection at a particular velocity to the projected area of the filter element. In Figure 18 the calculated γ, corresponding to the conditions given, is shown as a function of the Stokes number.

$$\gamma = \gamma_o N_{St}^{-2.54} \tag{17}$$

Yoshida and Tien (1985) showed that for aerosol filtration in granular beds, γ is proportional to $N_{St}^{-1.25}$. Their results were obtained, however, by fitting a large amount of experimental data collected by several investigators, some of which are shown in Figure 18. Fitting the data sets individually results in closer agreement of the exponent values.

Increase in collection due to aerosol loading

We used the experimental results of Emi et al. on the variation of the single-fiber efficiency with aerosol loading to make a comparison with the simulation predictions. The single-fiber efficiency η and the total collection efficiency of the model filter E are related by the expression

$$(1 - E) = \left(1 - \eta \frac{d_f}{\ell}\right)^2 \tag{18}$$

Accordingly, from the simulation and with the use of Eq. 18, the single-fiber efficiency η determined at various times can be used to determine the ratio η/η_o as collection proceeds. The loading effect on the increase in η can be seen by plotting $(\eta/\eta_o) - 1$ against m_d/m_0 as shown in Figure 19, where m_d is the surface loading (kg/m^2) defined as deposited particles per unit area of screen, and m_0 is the value of m_d corresponding to $\eta/\eta_o = 2$.

The use of the format of $(\eta/\eta_o) - 1$ against (m_d/m_0) was consistent with the correlation proposed by Emi et al., which is

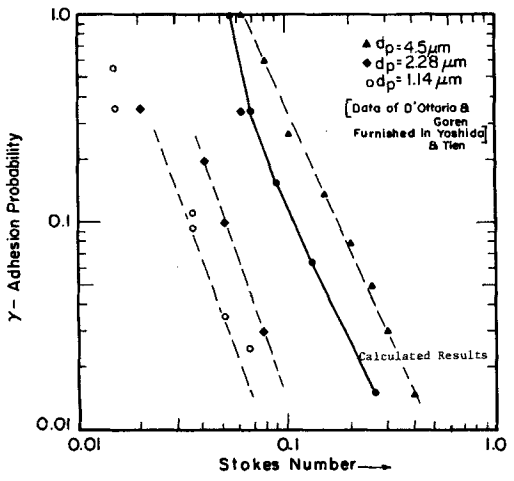

Figure 18. Adhesion probability variation with Stokes number.

Experimental data on bounce-off from granular filter beds
$d_p = 1$ μm; $d_f = 52.7$ μm; $\ell = 132$ μm

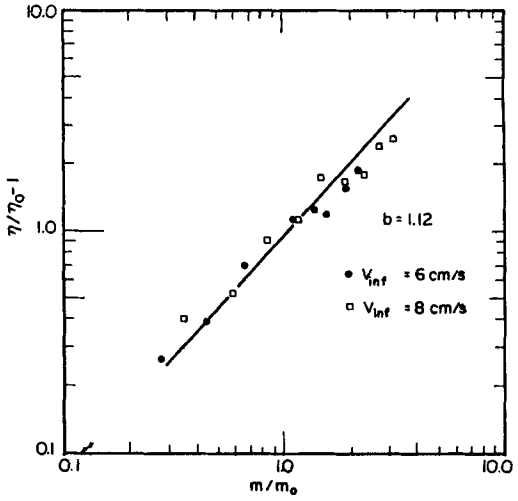

Figure 19. Variation of relative efficiency ratio with specific mass of deposits.

$m_o = c_o \eta_o V_\infty^{1/4}$; $d_p = 1$ μm; $d_f = 25$ μm; $\ell = 50$ μm

given as

$$\eta/\eta_o - 1 = (m_d/m_0)^b \tag{19}$$

$$m_o = c_o \eta_o V_{inf}^{1/4} \tag{20}$$

For the 500-mesh screens (consisting of fibers of 25 μm dia. and an interfiber distance of 49.5 μm) used by Emi et al., b was found to be 1.34, and m_0 (at $V_{inf} = 6$ cm/s) to be 5.89×10^{-4} kg/m^2. On the other hand, the simulation results give $m_0 = 1.75 \times 10^{-3}$ and the exponent $b = 1.12$. Thus, reasonably good agreement between simulation and experiment was observed.

Conclusions

We have set up a simulation of aerosol filtration in model fibrous filters consisting of layers of parallel fibers. This model simulated fibrous filters or wire-mesh screens. The effect of particle bounce-off, which earlier workers established to be an important factor influencing aerosol deposition in model fibrous filters, was accounted for appropriately.

The simulation results were analyzed and the effects of considering finite cross-sectional areas of the fibrous filters were examined. The statistical behavior of the collection efficiencies was also studied and the accuracy of the simulation established. The results of the simulation were used to analyze the particle trajectories within the filter and also to obtain a measure of the effect of varying such physical parameters as filter size and composition and aerosol particle velocity.

The simulation was applied to study particle deposition in model fibrous filters consisting of wire-mesh screens. Three aspects were considered: the initial collection efficiency of the meshes, the adhesion probability, and the change in collection efficiency due to deposition (or the loading effect). Comparisons between simulation and experiments in all three areas were made and surprisingly good agreement was observed when the particle inertia was high. These results suggest rather convincingly that at high particle inertia, bounce-off of impacting particles is a major factor in determining the rate of deposition of aerosols.

The present simulation serves two major purposes. It is a guide to experiments in deciding the major experimental variables of interest, and it serves to model the deposition process and its dependence on loading. The simulation gives us the three-dimensional structure of the deposits at any given time for given experimental conditions. The morphological characteristics of this deposit can be compared with those of the deposits found experimentally and can be applied to determine the validity of the basic principles we have used in the simulation. Comparing the simulation and the experimental results will help us to understand the development of aerosol deposits in fibrous filters and the eventual formation of the filter cake.

Notation

A = Hamaker constant, erg
c_o = constant reported by Emi et al. (1982)
d = diameter, μm
d_m = critical height for bounce-off, μm
e = coefficient of restitution
E = instantaneous collection efficiency
E_o = collection efficiency of a unit cell
E_w = magnitude of potential energy well due to surface interactions
k, v = appropriate functions of material properties, Table 1
KE = kinetic energy of particles, erg
ℓ = interfiber distance, μm
m = mass of a particle, g
m_d = mass of deposits
m_o = critical mass deposit, mass of deposit at which the increase in single-fiber efficiency η is 100% over η_o
n = number of deposited particles
N = number of particles approaching
N_{St} = Stokes number
V = velocity of particles, cm/s
Y = Young's modulus, dyne/cm^2
z_o = equilibrium separation distance

Greek letters

η = single-fiber collection efficiency
η_i = collection efficiency of each layer
η_o = single-fiber initial collection efficiency
μ = fluid viscosity, P
λ = inelasticity parameter
ρ = density of each material
γ = adhesion probability

Subscripts

cr = critical bounce-off condition
d = deposits
f = fiber
i = incident particle
n = normal component
p = particle
r = reflected particle
t = tangential component
∞, inf = free stream property
w = energy well

Literature Cited

Beizaie, M., C. S. Wang, and C. Tien, "A Simulation Model of Particle Deposition on Single Collectors," *Chem. Eng. Commun.*, **13,** 153 (1981).

Billings, C. E., "Effect of Particle Accumulation in Air Filtration," Ph.D. Diss., Calif. Inst. Technol., Pasadena (1966).

Dahneke, B., "The Capture of Aerosol Particles by Surfaces," *J. Colloid Interf. Sci.*, **37,** 342 (1971).

Davies, C. N., *Air Filtration,* Academic Press (1973).

Emi, H., C. S. Wang, and C. Tien, "Transient Behavior of Aerosol Filtration in Model Filters," *AIChE J.*, **28,** 397 (1982).

Jung, Y., S. A. Walata, and C. Tien, "Experimental Determination of the Initial Collection Efficiency of Granular Beds in the Inertial-Impaction-Dominated Regime," submitted *Aerosol Sci. Technol.* (1987).

Payatakes, A. C., and L. Gradon, "Dendrite Deposition of Aerosol Particles in Fibrous Media by Inertial Impaction and Interception," *Chem. Eng. Sci.*, **15,** 1083 (1980).

Payatakes, A. C., and C. Tien, "Particle Deposition in Fibrous Media with Dendritelike Pattern," *J. Aerosol Sci.*, **7,** 85 (1976).

Pendse, H., and C. Tien, "A Simulation Model of Aerosol Collection in Granular Media," *J. Colloid Interf. Sci.*, **87**(1), 225 (1982).

Tien, C., C. S. Wang, and D. T. Barot, "Chainlike Formation of Particle Deposits in Fluid Particle Separation," *Science,* **196,** 983 (1977).

Tsiang, R. C., C. S. Wang, and C. Tien, "Dynamics of Particle Deposition in Model Fiber Filters," *Chem. Eng. Sci.*, **37,** 1661 (1982).

Walata, S. A., T. Takahashi, and C. Tien, "Effect of Particle Deposition on Granular Aerosol Filtration," *Aerosol Sci. Technol.*, **5,** 23 (1986).

Wang, C. S., M. Beizaie, and C. Tien, "Deposition of Solid Particles on a Collector—Formulation of a New Theory," *AIChE J.*, **23,** 879 (1977).

Yoshida, H., and C. Tien, "A New Correlation of the Initial Collection Efficiency of Granular Aerosol Filtration," *AIChE J.*, **31,** 1752 (1985).

Manuscript received Oct. 15, 1986, and revision received July 20, 1987.